ARMY RESEARCH LABORATORY

Fusing Multiple Sensor Modalities for Complex Physiological State Monitoring

by Daniel Silversmith, Nicholas Perkons, Kesshi Jordan, Justin Brooks, William Hairston, Scott Kerick, Brent Lance, Kaleb McDowell, and William Nothwang

ARL-TR-6283 **December 2012**

Approved for public release; distribution unlimited.

NOTICES

Disclaimers

The findings in this report are not to be construed as an official Department of the Army position unless so designated by other authorized documents.

Citation of manufacturer's or trade names does not constitute an official endorsement or approval of the use thereof.

Destroy this report when it is no longer needed. Do not return it to the originator.

Army Research Laboratory
Adelphi, MD 20783-1197

ARL-TR-6283 **December 2012**

Fusing Multiple Sensor Modalities for Complex Physiological State Monitoring

Daniel Silversmith, Nicholas Perkons, Kesshi Jordan, and William Nothwang
Sensors and Electron Devices Directorate, ARL

Justin Brooks, William Hairston, Scott Kerick, Brent Lance, and Kaleb McDowell
Human Research Engineering Directorate, ARL

Approved for public release; distribution unlimited.

REPORT DOCUMENTATION PAGE

Form Approved
OMB No. 0704-0188

Public reporting burden for this collection of information is estimated to average 1 hour per response, including the time for reviewing instructions, searching existing data sources, gathering and maintaining the data needed, and completing and reviewing the collection information. Send comments regarding this burden estimate or any other aspect of this collection of information, including suggestions for reducing the burden, to Department of Defense, Washington Headquarters Services, Directorate for Information Operations and Reports (0704-0188), 1215 Jefferson Davis Highway, Suite 1204, Arlington, VA 22202-4302. Respondents should be aware that notwithstanding any other provision of law, no person shall be subject to any penalty for failing to comply with a collection of information if it does not display a currently valid OMB control number.
PLEASE DO NOT RETURN YOUR FORM TO THE ABOVE ADDRESS.

1. REPORT DATE *(DD-MM-YYYY)*	2. REPORT TYPE	3. DATES COVERED (From - To)
December 2012	Final	June 1, 2011 to September 1, 2012

4. TITLE AND SUBTITLE
Fusing Multiple Sensor Modalities for Complex Physiological State Monitoring

5a. CONTRACT NUMBER

5b. GRANT NUMBER

5c. PROGRAM ELEMENT NUMBER

6. AUTHOR(S)
William Nothwang, Daniel Silversmith, Nicholas Perkons, Kesshi Jordan, Justin Brooks, William Hairston, Scott Kerick, Brent Lance, and Kaleb McDowell

5d. PROJECT NUMBER

5e. TASK NUMBER

5f. WORK UNIT NUMBER

7. PERFORMING ORGANIZATION NAME(S) AND ADDRESS(ES)
U.S. Army Research Laboratory
ATTN: RDRL-SER-L
2800 Powder Mill Road
Adelphi, MD 20783-1197

8. PERFORMING ORGANIZATION REPORT NUMBER
ARL-TR-6283

9. SPONSORING/MONITORING AGENCY NAME(S) AND ADDRESS(ES)

10. SPONSOR/MONITOR'S ACRONYM(S)

11. SPONSOR/MONITOR'S REPORT NUMBER(S)

12. DISTRIBUTION/AVAILABILITY STATEMENT
Approved for public release; distribution unlimited.

13. SUPPLEMENTARY NOTES

14. ABSTRACT
Both the public sector and the military are working on developing drowsiness detection systems, as driver fatigue is a significant contributor to motor vehicle accidents. Individually, electroencephalography (EEG) and eye-tracking measures are tenuous indicators of driver fatigue and impairment. This project proposes to integrate multiple sensor modalities in order to improve drowsiness level assessment and driver performance prediction. There is substantial evidence supporting the correlation of alpha bursts in EEG (narrowband alpha power density increases lasting 500 ms to several seconds) and eye-tracking measures, such as pupil diameter and gaze distribution, with drowsiness. As a step towards multi-sensory data fusion, we aim to implement in real time an optimized version of an existing algorithm for the automatic detection of alpha bursts using a single EEG channel and ascertain correlations between alpha bursts, eye-tracking measures, and behavioral indicators of fatigue that include standard deviation of both lane position and acceleration. The ability to reliably detect alpha bursts in real-time combined with established correlations will allow an algorithm to accurately predict driver performance in a simulation environment.

15. SUBJECT TERMS
Alpha burst, electroencephalography (EEG), drowsiness, eye-tracking

16. SECURITY CLASSIFICATION OF:			17. LIMITATION OF ABSTRACT	18. NUMBER OF PAGES	19a. NAME OF RESPONSIBLE PERSON
a. REPORT	b. ABSTRACT	c. THIS PAGE			William Nothwang
Unclassified	Unclassified	Unclassified	UU	38	19b. TELEPHONE NUMBER (*Include area code*) (301) 394-1163

Standard Form 298 (Rev. 8/98)
Prescribed by ANSI Std. Z39.18

Contents

List of Figures

List of Tables

1. Introduction

1.1 Problem Statement (Driving – Drowsiness Causes Crashes)

The significant role of drowsiness in motor vehicle accidents is a serious concern for both the public sector and the military. In 1990, the U.S. National Transportation Safety Board (NTSB) determined fatigue to be the most frequent factor in U.S. fatal truck crashes (*1*). Another NTSB study in 1995 found that 58% of the 107 non-fatal single-vehicle roadway departure truck crashes were related to fatigue (*2*). Dinges et al., cites that fatigue can be at least partially attributed to 2%–23% of all crashes (*3–7*), 4%–25% of single-vehicle crashes (*8, 9*), 10%–40% of long motor way crashes (*10, 11*), and 15% of fatal single-vehicle truck crashes (*8*).

Studies on the incidence of drowsiness-related motor vehicle accidents indicate that drivers are generally ineffective in judging performance degradation due to drowsiness until they are severely impaired to the point of head bobbing (*12*). This indicates that real-time drowsiness detection systems are needed for the typical driver to enhance their ability to judge drowsiness onset.

1.2 Objective of this Project

Defining the drowsiness state is subjective and beyond the scope of this report. Rather than attempting to assess drowsiness, this report reflects a portion of a larger project proposing to fuse multiple sensor modalities in order to predict fatigue-induced driver performance through the integration of electroencephalography (EEG), eye-tracking sensors, and behavioral monitors. As an initial step towards the prediction of driver performance degradation as a result of drowsiness, the work described in this report aims to complete the following two objectives:

1. Implement an improved, fieldable algorithm for the automatic detection of alpha bursts. *(Accomplished)*
2. Quantify cross-correlations between eye-tracking features, alpha bursts, and fatigue-related driver performance measures. *(Partially Accomplished)*

This report describes the methodologies we employed to accomplish the automatic detection of alpha bursts in EEG, the eye-tracking analysis, the behavioral analysis, and the cross sensor correlation analysis. This report also highlights the effectiveness of using these methods, discussing the reasons that some of the methods used were ineffective within this particular implementation.

1.3 State of the Art Fatigue Systems

Several real-time drowsiness monitoring systems have been, or are in the process of being, developed, but the technology has not yet reached an acceptable level of accuracy for the Army.

This is due in a large part to the difficulty in defining the abstract concept of "drowsiness" in clinically measurable terms. Some promising technologies for predicting behavioral performance indicators of drowsiness are EEG, eye-tracking measures, and driver performance. Each of these sensor modalities has been individually correlated to the state of drowsiness. Spectral power has a characteristic distribution in EEG recordings of the parietal and occipital regions of the brain during the drowsiness state as compared to REM sleep and other states, as seen in figure 1 (*13*). Furthermore, using EEG, Picot et al. (*14*) were able to achieve 85% sensitivity and 20% specificity in assessing drowsiness. PERCLOS of the eye, defined as the percentage of time the eye is at least 80% closed, has been highly correlated to drowsiness; it yields a 20-min bout-to-bout coherence Pearson correlation coefficient of 0.878 (*15*). The eye-tracking measures of pupil constriction and oscillation are also valid measurements for drowsiness detection (*16*). Many vehicle-based drowsiness detection systems use behavioral measures, such as standard deviation of lateral lane position (STDLAT), to assess sleepiness. STDLAT has been correlated to the Karolinska Sleepiness Scale (KSS), with a chi-squared value of 11 ($p < 0.001$) (*17*). For this study, we look at the cross correlation of behavioral, eye-tracking, and EEG as a means to understanding how multiple sensor modalities can be used to improve the sensitivity and specificity of drowsiness prediction.

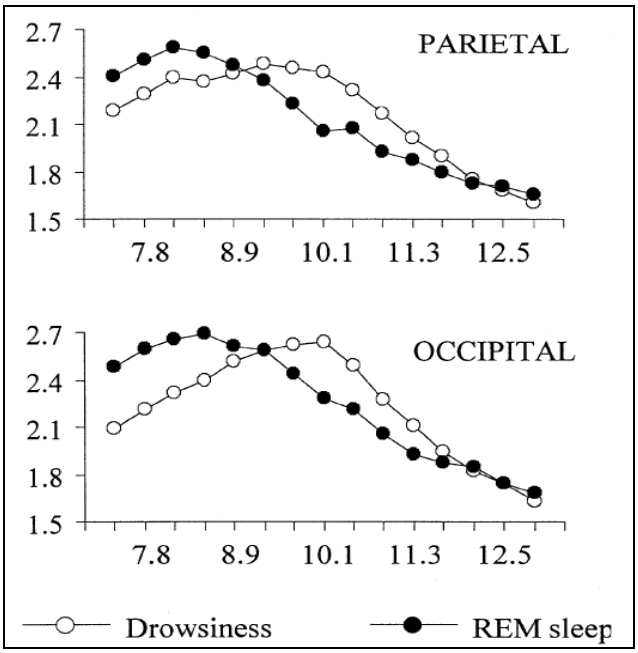

Figure 1. Spectral power contribution of sleep-alpha variants (drowsiness alpha activity and REM-alpha bursts) over frontal, central, parietal and occipital regions. Note the higher spectral contribution of the slowest components (7.8–8.6 Hz) during REM alpha bursts as compared with drowsiness-alpha activity (*13*).

1.4 EEG—Definition and Relation to Drowsiness

EEG is the study of the electrical signals generated by the human brain. Most notable to the field of electroencephalography, an electroencephalogram is a device that simultaneously records the voltage across a reference electrode (or set of reference electrodes) and many additional individual electrodes, all positioned on a subject's scalp. Since its initial use in 1929, physiologists have inferred that an EEG's electrical readings are a measure of the electrical activity of the brain (*18*). The changes in electrical potential of a particular electrode over time have been interpreted as the temporal changes in neurological response, which spatially correspond to a specific region of the brain. The distribution of electrodes over the scalp provides a means for comparison of neurological responses in different regions of the brain at a particular instance in time. Most current, lab-based systems EEG devices consist of 16–256 electrodes snapped into a form-fitting cap placed on the subject's head, and require conducting gel to facilitate an electrical connection between the scalp and the electrodes. Systems designed for gaming tend to have even fewer electrodes and many utilize dry electrode technology.

1.5 Current EEG Analysis Approaches to Measure Drowsiness

Recent research has explored the correlation of EEG signals with behavioral indicators of drowsiness. Studies have found that the onset of drowsiness is typically associated with an increase in brain activity in the alpha and theta frequencies (8–13 and 4–7 Hz, respectively) coinciding with a decrease in brain activity in the beta band (14–60 Hz) (*18*, *19*).

EEG recordings from subjects participating in a driving simulation were obtained to assess the viability of using a means comparison test to monitor the $(\alpha + \theta)/\beta$ ratio as a drowsiness detection algorithm (*14*). This method did not predict driver performance; instead, this algorithm attempted to assess whether or not a subject was drowsy. The algorithm's output was compared to an expert's drowsiness assessment of many 20-s EEG segments, boasting 85% sensitivity and 20% specificity for assessing drowsiness. The main advantage of this algorithm is that it can be run in near real time on a single EEG channel, making it a fieldable algorithm. However, this algorithm is limited in that it attempts to assess the complex physiological state of drowsiness. Furthermore, power ratios are not ideal indicators for detecting fatigue due to the detrimental effects that artifacts and noise—which are present in field environments—have on these metrics (*20*).

Simon et al. (*20*) proposed that the detection of alpha bursts is a more robust measure of fatigue in the presence of artifacts. Alpha bursts (pictured in figure 2) are characterized by narrowband increases in power within the alpha frequency band (8–13 Hz) and are typically observed in a subject's EEG signal when transitioning between drowsiness and the early stages of sleep (*14, 19, 21*). Simon et al. compared alpha burst frequency and alpha power in subjects during a real driving task. The frequency of alpha bursts increased by 90% from the awake to drowsiness states whereas alpha power only increased by 32%. The findings indicate that alpha burst detection provides a more accurate drowsiness assessment than power measures under real

driving conditions. The main advantage of this algorithm is that it uses a single EEG channel and is relatively robust in the presence of noise and artifacts. However, this algorithm does not work in real time and is, therefore, not field-implementable. In this study, we avoided the issue of defining the drowsiness state. Instead, we accepted that alpha burst frequency is a robust indicator of the transition between being awake and asleep and intended to improve upon the Simon et al. alpha burst detection algorithm by implementing it in real time and optimizing its parameters (*20*).

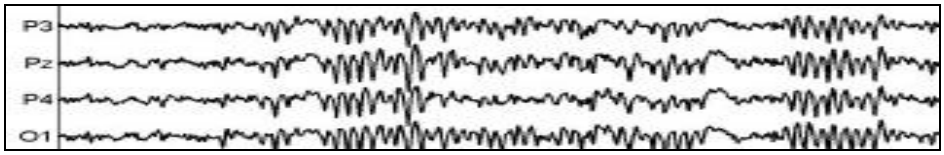

Figure 2. Example of alpha burst in the parietal and occipital regions of the brain (*20*).

1.6 Eye-tracking

Recent advancements in eye-tracking technology have enabled the eye to be monitored remotely, making this device the least intrusive. Eye-tracking techniques usually consist of a table or dashboard mounted camera with software that uses feature extraction for each image to record measures such as PERCLOS, pupil diameter, and gaze distribution (GAZEDIS). As shown in figure 3, there has been a substantial amount of causal interaction research that has linked a number of different exposures to potential fatigue outcomes (*22*). Ji et al. (*22*) have used this to develop a statistical Bayesian Network causal relationship between exposure and outcome.

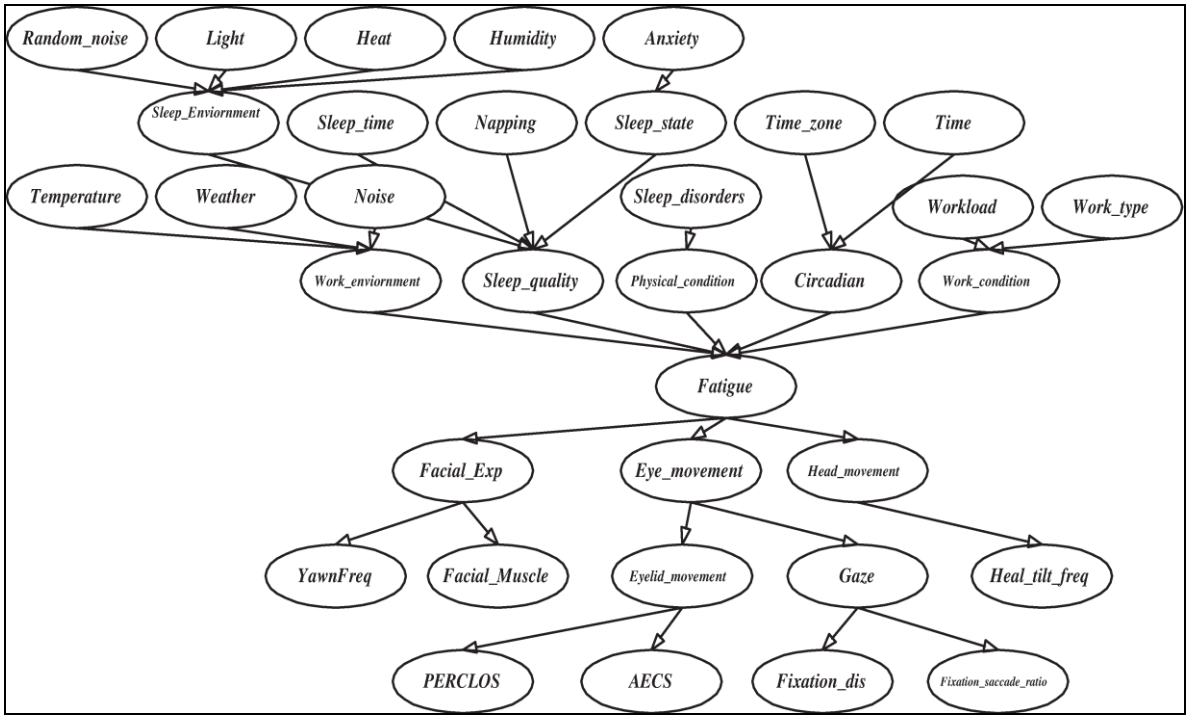

Figure 3. Work by Ji et al. (*22*) highlighting the causal interactions and outcomes regarding fatigue.

1.7 Current Eye-tracking Systems to Measure Drowsiness

Drowsiness is an inherently difficult physiological construct to experimentally define. Many researchers, instead, correlate behaviors or physiologically measurable factors to outcomes, thus obviating the need to strictly define "drowsiness." The Federal Highway Administration has determined the most effective measure of alertness, the inverse of drowsiness, to be PERCLOS—defined as the percentage of the time that the eye is at least 80% closed (*1*). A Department of Transportation study strongly correlated PERCLOS with psychomotor vigilance test (PVT) performance lapses, which is a well-documented good test for driving alertness performance measure (*15*). More specifically, PERCLOS is defined as the percentage of time within a minute that the eye is more than 80% closed (*23*) and is considered the gold standard for measuring alertness (*24*). The disadvantage to using PERCLOS as a real-time drowsiness measure is that calculating PERCLOS requires a time-delay on the order of minutes. Any time-delay decreases the efficacy of a fielded drowsiness monitoring system, as driver impairment feedback notification will be delayed as well. An incident caused by drowsiness-related impairment could occur in the minutes required to process the PERCLOS data; however, except in extreme cases, most people do not experience drastic changes in alertness over a few seconds. Instead, most people experience a gradual change over many minutes from alert to not alert. As such, PERCLOS measures that have a measurement time of several minutes should be applicable for most driving-based applications.

Many additional eye-tracking measures have been investigated as indicators of drowsiness, including pupil diameter, GAZEDIS, and saccadic velocity. The study by Merritt (*16*) found that measures of pupil constriction and oscillation were valid metrics for this application. Russo et al. (*25*) found a correlation between simulation car crash incidence with decreases in saccadic velocity (R^2 = 77%) and increases in pupil constriction latency (R^2 = 88%). Jain et al. (*26*) used the sum of spectral power from 0 to 0.8 Hz of pupil diameter for 82-s windows as a measure of "pupillary unrest" (effect size = 0.9). In this study, we investigated cross correlating the eye-tracking features of pupil diameter and gaze distribution, since these measures can be calculated almost instantaneously. Since drowsiness comes in cycles with both low and high frequency components (*2, 27*), we investigated both short term (minute-to-minute) and long term (10 min bout-to-bout) time intervals. A high degree of both inter- and intrapersonal variation in these correlates has been previously established (*1, 28*), so we conducted a variation study both within subject datasets and between subject datasets.

1.8 Behavioral Indicators of Fatigue

A number of driving performance measures have been established as drowsiness-related. A very commonly used metric is lane drifting, measured by the SDLAT (*2, 29*). A linear trend of the SDLAT as a function of the KSS yielded the chi-squared value of 38 ($p < 0.001$) with an average increase of 0.032 m for each level of the KSS (*28*). Adding a squared component further improved the model fit (chi-squared value is 11, $p < 0.001$), suggesting a curvilinear relationship

between the KSS and SDLAT (*25*). Reaction time is also a very important driving performance factor (*30*) that is highly correlated to drowsiness (*31*). In this study, we investigated the drowsiness measures SDLAT and standard deviation of acceleration.

In addition, we investigated the drowsiness measures SDLAT and standard deviation of acceleration because these measurements were continuous rather than event-specific metrics, and they provided enough data for comparison with other sensor modalities. Reaction time was rejected as a viable measure of drowsiness in this case, because measurements of reaction time occurred at discrete events that often did not overlap with alpha bursting or "good" windows of eye-tracking data; therefore, statistically significant analysis using reaction time could not be performed on the limited dataset (*32*). Instead, we explored the possibility of using the standard deviation of acceleration as a substitute for reaction time analysis. Although this metric has not been correlated with drowsiness, we assumed that standard deviation of acceleration can be interpreted as a continuous measure of a driver's instantaneous reaction to random deviations from the target speed.

2. Methodology

In order to accomplish our objectives, two distinct phases of the project were realized, depicted in figure 4. The initial data from each of the three sensor modalities were pre-processed, parsed, and ground-truthed. Once this pre-processing was finished, an alpha burst detection algorithm with the ability to be implemented in near real time was performed post-hoc on the data and improved through optimization. Concurrently, correlations between the different sensor modalities were established and quantified.

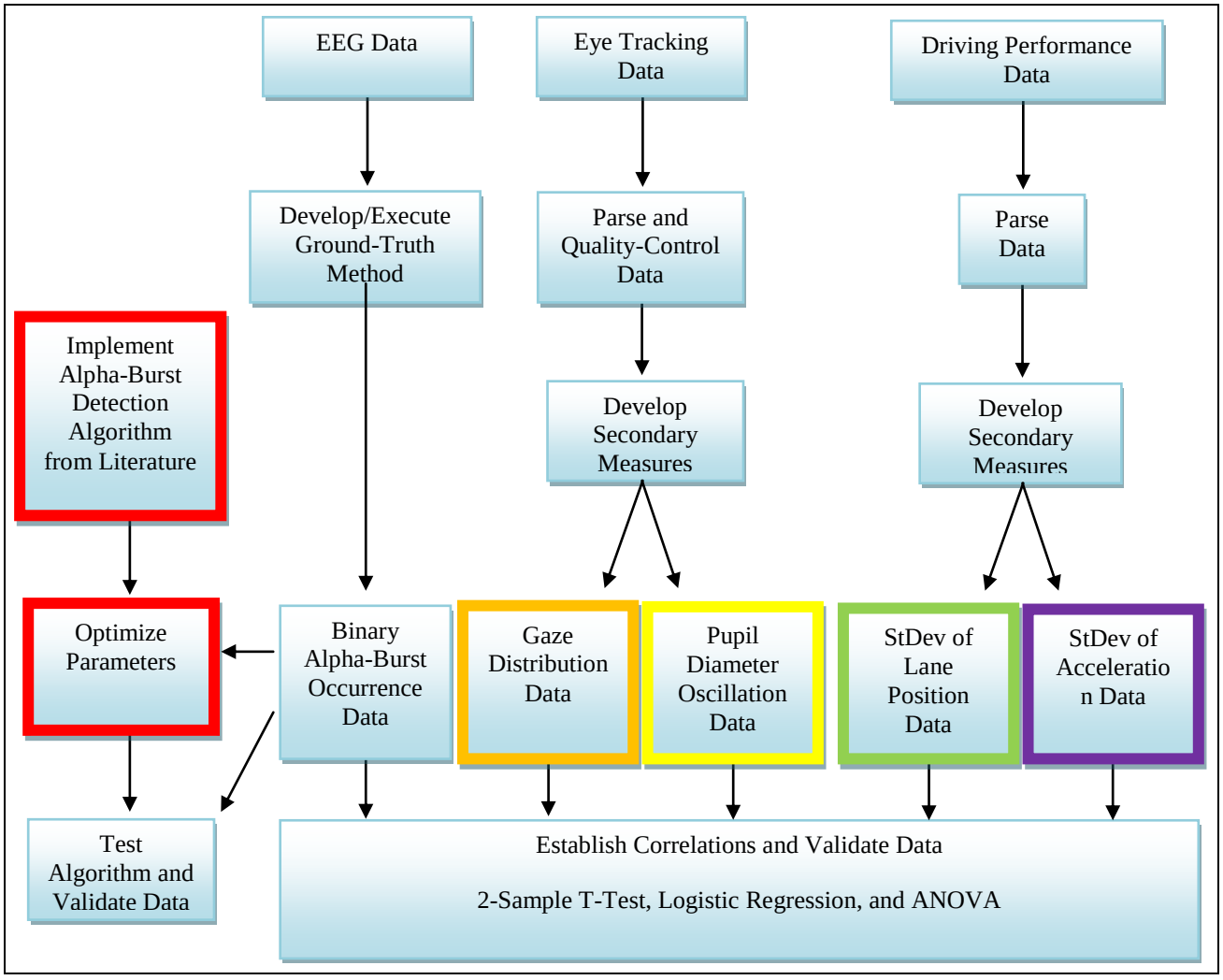

Figure 4. This overarching project map depicts the relationships between three branches of sensor data: EEG, eye-tracking, and driving performance.

2.1 Driving Simulation

The data used in this report were taken from a Driving Simulation Pilot Experiment performed by the Human Research and Engineering Directorate (HRED) of the U.S. Army Research Laboratory in summer 2012 at Aberdeen Proving Grounds, MD. Twenty-three male subjects participated in the experiment. The simulation consisted of a driving task for which participants were asked to drive straight for a period of 45 min to 1 hour after a 15-min calibration drive. The simulator consisted of a video game mock-up of a racecar wheel that controlled the virtual movements of the subject's car on a computer monitor. A representation of the simulation field of view is shown in figure 5. The simulator also recorded various driver activity metrics, including lane position, speed, and acceleration. Periodically throughout the experiment, the simulator delivered a "perturbation event," which caused a virtual disturbance in the heading of the subject's vehicle. The amount of time the subject took to initialize a response is referred to as the perturbation event "reaction time" in the analysis.

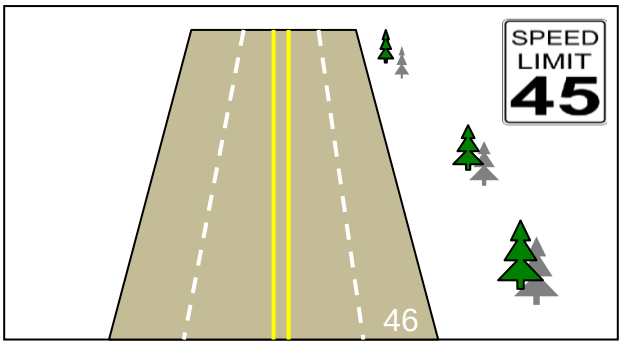

Figure 5. Representation of the simulation field of view.

2.2 Automatic Detection of Alpha Bursts

2.2.1 BioSemi System

Throughout the driving simulation, the subject's brain activity was monitored via a BioSemi EEG system (figure 6). The EEG hardware used in this study consists of 64 active channels and 8 additional channels, which include electrooculography (EOG) channels and reference electrodes. Each channel recorded data, which were analyzed post-simulation using Matlab and the EEGLab toolbox (*33*).

Figure 6. The 64-channel BioSemi EEG System (*33*).

2.2.2 Establishing Ground Truth

In order to implement a fieldable algorithm to detect alpha bursts, a means of assessing the algorithm needed to be established. There was no standard protocol for identifying alpha bursts. Rather, an EEG expert is needed to manually identify "events" from EEG features. Part of the scope of this report includes the development of a standardized protocol for establishing ground truth for EEG features. The procedure for establishing ground truth is outlined here:

1. Using a scale from 0–3 (0: No, 1: Maybe, 2: Probably, 3: Textbook Example), two independent reviewers examine all of the EEG data and record the start and end times of regions corresponding to alpha bursts, according to the following criteria:

- Presence of medium to high amplitude activity in the alpha range (8–13 Hz) located in the occipital and parietal lobes
- Duration of at least 0.5 s
- Alpha bursts separated by 1 s or less are combined into a single burst

2. The two independent reviewers meet and examine all examples rating disagreements resulting from step one, deciding upon the absolute binary presence or absence of an alpha burst for each event. Any event with a score of 1 or 0 is eliminated from the dataset.
3. The final list of alpha bursts for 80% of the subjects is sent to an expert (EEG neuroscientist with 10+ years of experience) for final review and to eliminate false positives. The expert then blindly reviews the remaining 20% of subjects to establish a false negative rate.

The implementation of Step 3 in the procedure was reduced from 80% of all subjects to one subject (4.3%) in the initial implementation and will be expanded to the full percentage in the final experimental implementation.

2.2.3 Original Algorithm

To ascertain the correlation between alpha bursts and drowsiness, Simon et al. developed an algorithm for the automatic detection of alpha bursts. A flowchart representation of this algorithm is pictured in figure 7. To estimate the characteristic ($1/f^{-\beta}$) noise in the EEG signal, the algorithm applied an exponential fit to the amplitude spectral density (ASD) of each subject's entire recording (*20*, *34*). The algorithm epoched (discretely segmented) the data for each EEG channel into 1-s windows with an overlap of 750 ms across windows. To negate the effects of windowing the data, each window was zero-meaned and multiplied with a Hamming window. The short time Fourier transform (in its fast Fourier transform implementation) was computed to ascertain the spectral amplitude density in each window. The previously calculated noise approximation was applied to the current segment by multiplying the exponential curve by the ratio of the integrated mean spectrum of the current window to the integrated mean spectrum of the entire recording. The full width at half maximum (FWHM) of the alpha frequency peak was then calculated according to the following procedure. First, the two local minima surrounding the peak were located. From there, the "bottom" of the peak was calculated by averaging the amplitude of the local minima. The FWHM was considered to be the width of the peak at the height midway between the "bottom" and maximum of the peak. If the characteristics of the window met the following criteria, the window was said to contain an alpha burst:

1. The peak ASD was in the alpha frequency band (7–13 Hz).
2. The FWHM of the peak ASD was less than half the bandwidth of the Hamming window.

3. The area in the peak ASD above the noise estimate (signal) was greater than the area in the peak ASD below the noise estimate (noise).

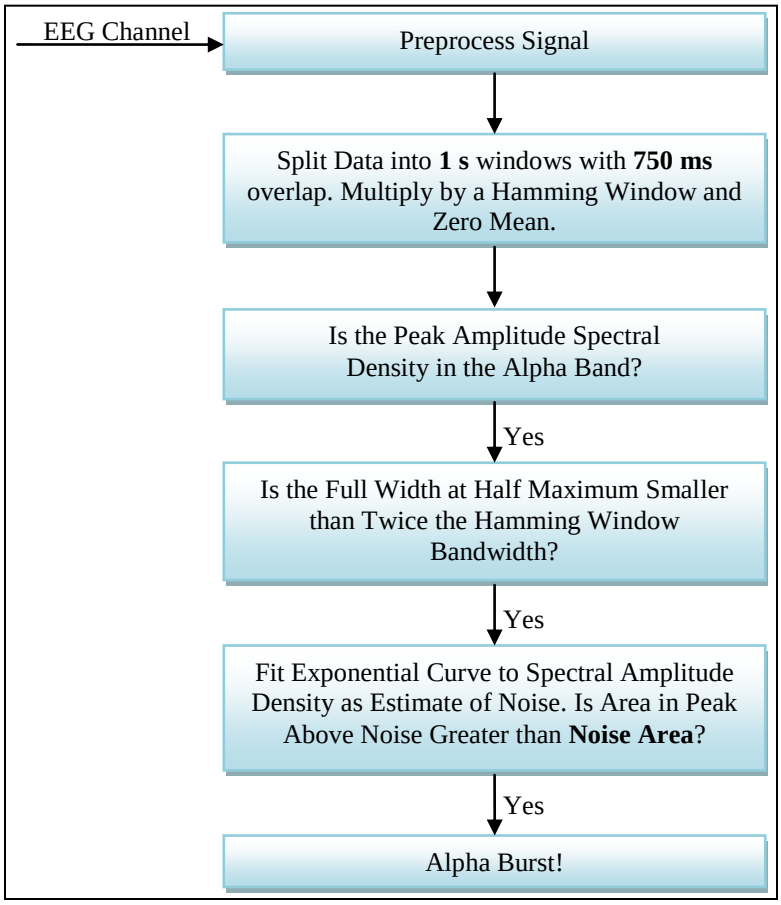

Figure 7. Algorithm for automatic detection of alpha bursts (*20*).

2.2.4 Fieldability Concerns

Simon et al., in (*20*) attempted to address the fieldability concerns of using EEG by only requiring a single channel as input for this alpha burst detection algorithm. It is important to note, however, that the noise estimation portion of Simon et al.'s algorithm could not be implemented in real time since it required the entire EEG recording. Although Simon et al. partially addressed the fieldability concerns of using EEG as a drowsiness detector, a crucial step of the proposed algorithm was to estimate the noise across the frequency spectrum in the EEG signal. Simon et al. applied an exponential fit to the mean spectral amplitude density for the entire recording in each channel in order to approximate the nonlinear ($1/f^{-\beta}$) noise that is inherent in EEG recordings (*29*). This curve acted as a barrier allowing one to distinguish between the signal (the spectral amplitude density above the curve) and the inherent EEG noise (the spectral amplitude density below the curve). In order to account for inter-subject and longitudinal noise variability, Simon et al. multiplied the noise estimation by the ratio between the integrated spectrum of the current window with the mean integrated spectrum of the entire recording. Since this noise

estimation scheme required post-processing of the entire recording, the algorithm outlined by Simon et al. could not be performed in real time.

In order to implement a near-real-time alpha burst detector, the noise approximation scheme described by Simon et al. was adjusted. Rather than fitting an exponential curve to the entire recording and then applying a proportional curve to each window, as Simon et al., did, an exponential curve was instead fitted to each window independently. An example window of the real-time implementation of the alpha burst detection algorithm is shown in figure 8.

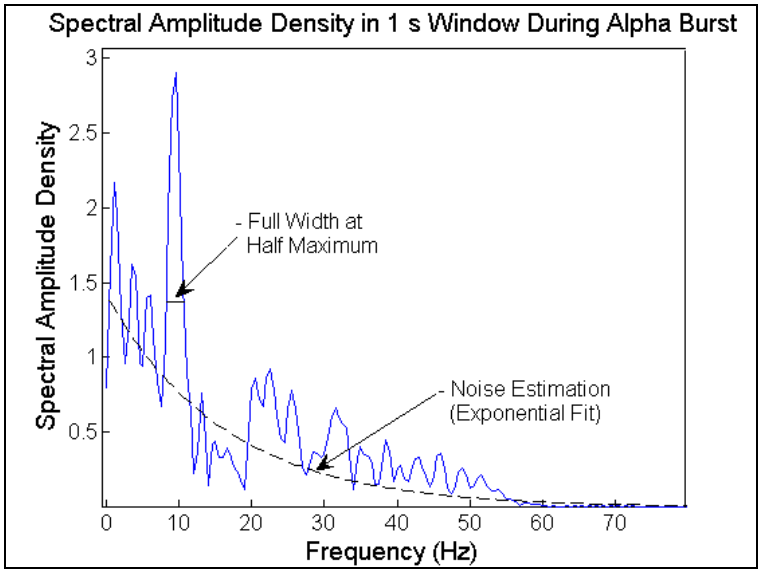

Figure 8. Depiction of the spectral amplitude density of a one-second window during an alpha burst. The real-time noise approximation overlays the spectral amplitude density.

2.2.5 Algorithm Optimization

To improve the real-time implementation of the alpha burst detection algorithm, the EEG data was split into three subsets: a training dataset, a testing dataset, and a validation dataset (about 70%, 20%, and 10% of the data, respectively). The EEG recordings from each subject were split into segments of roughly 100 s and randomly distributed into each dataset. The training dataset was used to choose the optimum channel and optimize the algorithm. The first step of the algorithm optimization procedure was to run the real-time implementation of the alpha burst detection algorithm for all 64 channels within the training dataset. Then the sensitivity (true positive rate) and specificity (true negative rate) were assessed for each channel using ground-truth data. Treating the sensitivity and specificity scalar values as orthogonal vectors allowed us to find the optimal channel. The optimal channel had the minimum distance between the vector <sensitivity, specificity> and the vector <1, 1>. Once the optimal channel was discovered, the remaining optimization was specific to that channel.

Multiple parameters were independently optimized by running the alpha burst detection algorithm on the best channel while varying the values of each parameter—one parameter at a time. The sensitivity and specificity were calculated for each value of each parameter using the training dataset. The same technique described for finding the optimal channel was used for each parameter; the optimal value for the current parameter was discovered by finding the value that yielded the minimum distance between the vector <sensitivity, specificity> and the vector <1, 1>. This procedure was performed for the following parameters: window length, overlap between windows, minimum alpha frequency, and maximum alpha frequency.

2.2.6 Testing and Validation

Once the optimum values for each parameter were found, three iterations of the alpha burst detection algorithm were tested: the original algorithm, the real-time implementation of the algorithm with original parameters, and the real-time implementation of the algorithm with optimized parameters. For each iteration of the algorithm, the sensitivity and specificity were calculated using the testing dataset.

A third dataset, the validation dataset, was used to verify that the training and testing datasets were representative of all the alpha burst data. To verify that the three datasets were statistically equivalent, we performed multiple two-sample hypothesis t-tests on the frequency of alpha bursts in each dataset. We tested the null hypothesis that the frequency of alpha bursting in the training and validation sets, as well as the testing and validation sets, were equivalent.

2.3 Eye-tracking

2.3.1 SensorMotoric Instruments Eye-tracking System

The subject's eye movements were recorded by the SensoMotoric Instruments Eye-tracking System with sampling rate of 250 Hz and spatial resolution of 0.03°. This eye-tracking system remotely records the right- and left-eye-mapped pupil diameters (RmapD and LmapD), and the gaze measure x-y point-of-regard (PORx and PORy) in real time using a camera mounted on the simulator. Pupil diameter and point-of-regard data can be examined using plots such as the ones in figures 9 and 10, respectively. In figure 9, the horizontal plane represents the subject's field of view. A frequency plot of viewed x-y coordinates reveals how the gaze was distributed across the field of view during a given time interval. In this case, the gaze is concentrated in the upper middle region of the simulation screen. In figure 10, both low and high frequency components are apparent in the temporal plot (time in sec) of pupil diameter (mm). Pupil diameter data are often examined in the frequency spectrum rather than the temporal domain.

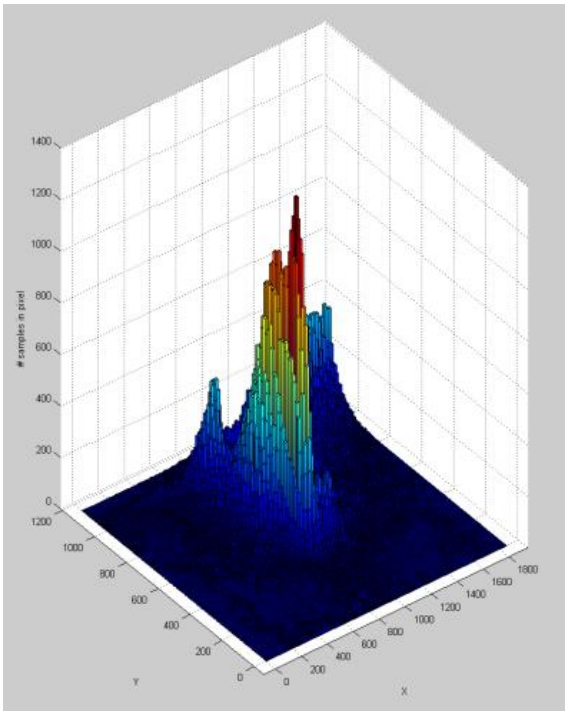

Figure 9. Gaze distribution of the eye on a 2-D screen. The horizontal plane represents the subject's field of view. A frequency plot of viewed x-y coordinates reveals how the gaze was distributed across the field of view during a given time interval.

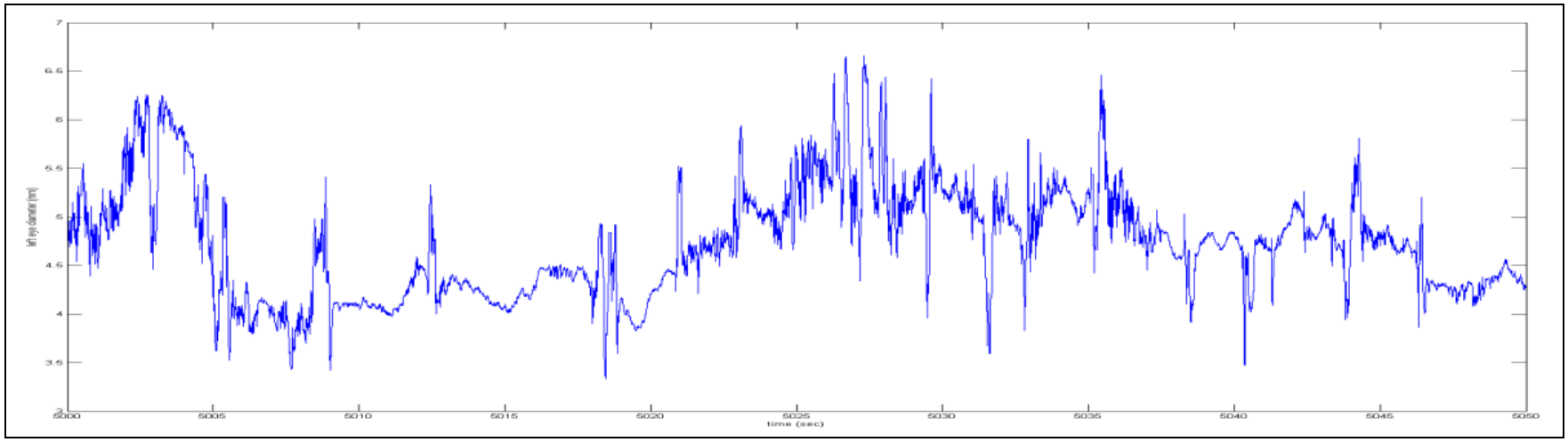

Figure 10. Pupil diameter (mm) over time (s).

2.3.2 Pupil Diameter

Eye-tracking was measured as "pupillary unrest" similar to the study in reference 26. The data were interpolated to 250 Hz and the DC offset eliminated by subtracting the mean from each data point. Next, the data were separated into 5-s windows. The FFT and power spectrum were calculated, and the spectral power between 0 and 0.8 Hz was measured for each window independently. Windows with gaps greater than two samples (assuming 250 Hz) were labeled as "bad windows" and were rejected from analysis. Figure 11 illustrates the pupil diameter data processing.

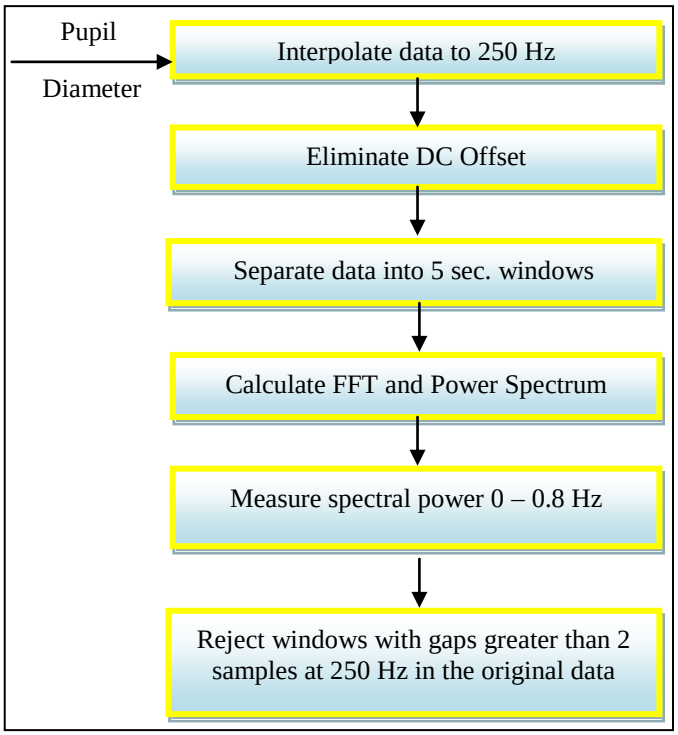

Figure 11. Flowchart of pupil diameter data processing.

2.3.3 Gaze Distribution

Gaze distribution was measured with a velocity-based metric. The average velocity of the eye's (x,y) point-of-regard was calculated for every 5-s window. This method was selected to minimize the effects of differing strategies of completing the simulation. The visual field actually required to successfully complete the simulation was very small, as the speedometer was placed on top of the road itself, and no complex maneuvers requiring foresight were required. Fixations on a particular area of interest could be indicative of the way that the subject chose to complete the simulation (simply staring at the speedometer and focusing on maintaining the exact speed), or of actual drowsiness affecting their gaze distribution. This factor was not controlled for, so the velocity-based metric does not favor a fixation at any single point on the screen, but is rather a representation of the eye's overall movement. Both methods would be confounded by this simulation design, but the velocity-based method averaged across windows minimizes its effect.

For quality-control of the data, all (0,0), (x,0), and (0,y) points were removed, as they represented missing data points in the dataset due to the gaze leaving the simulation field of view or the camera losing sight of the pupil. Next, intervals with a sampling rate ranging from 240–260 Hz were used exclusively to minimize error due to non-uniform sampling. This data were separated into 5-s windows and synced to windows established in the pupil diameter data. The average velocity of the point of regard was returned for each window, and then windows with less than 20% of the mean window sample size were labeled as "bad windows" and were rejected from analysis. Figure 12 illustrates the gaze distribution data processing.

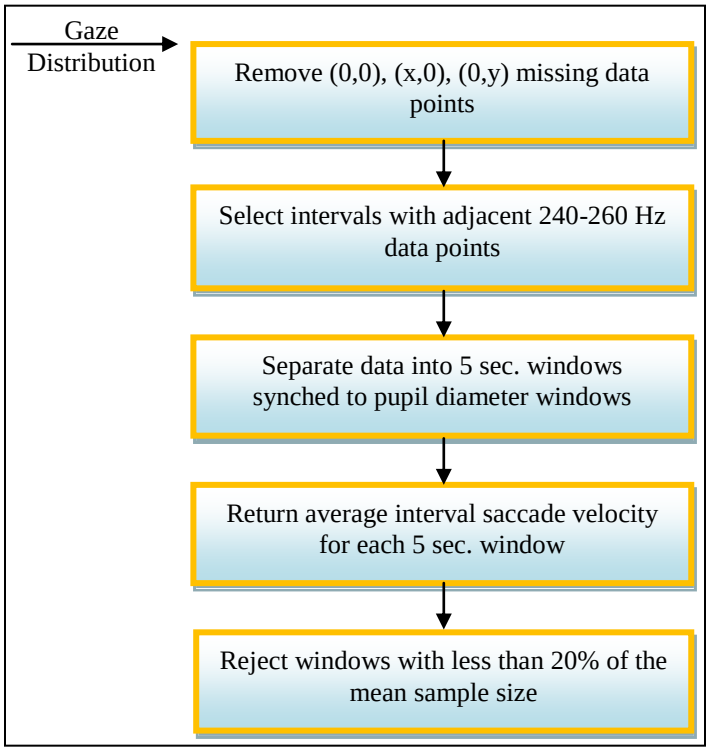

Figure 12. Flowchart of gaze distribution data processing.

2.4 Behavioral Indicators of Fatigue

Behavioral data, recorded at 90–100 Hz, were provided by the Driving Simulation and contained information regarding the state of the vehicle in the simulation at a given point in time. The driver performance metrics recorded by the simulator included X and Y coordinates, speed, and acceleration. In addition, the simulation generated a perturbation that distorted the heading of the vehicle at evenly distributed intervals, which the driver had to correct for. The reaction time of the driver provided an additional behavioral metric to analyze.

In order to classify this behavioral driving data, we analyzed them using two different procedures: the first methodology used regularly spaced windows and the second methodology separated data into discrete, event-specific windows. The continuous window approach involves analysis of driver performance metrics, including standard deviation of lane position and

standard deviation of acceleration, in continuous windows for the duration of the experiment. The discrete, event-specific approach involves analysis of driver performance metrics in the window of time surrounding a specific event, in our case the reaction time to a perturbation generated by the simulation. For a graphic depiction of the two approaches, see figure 13.

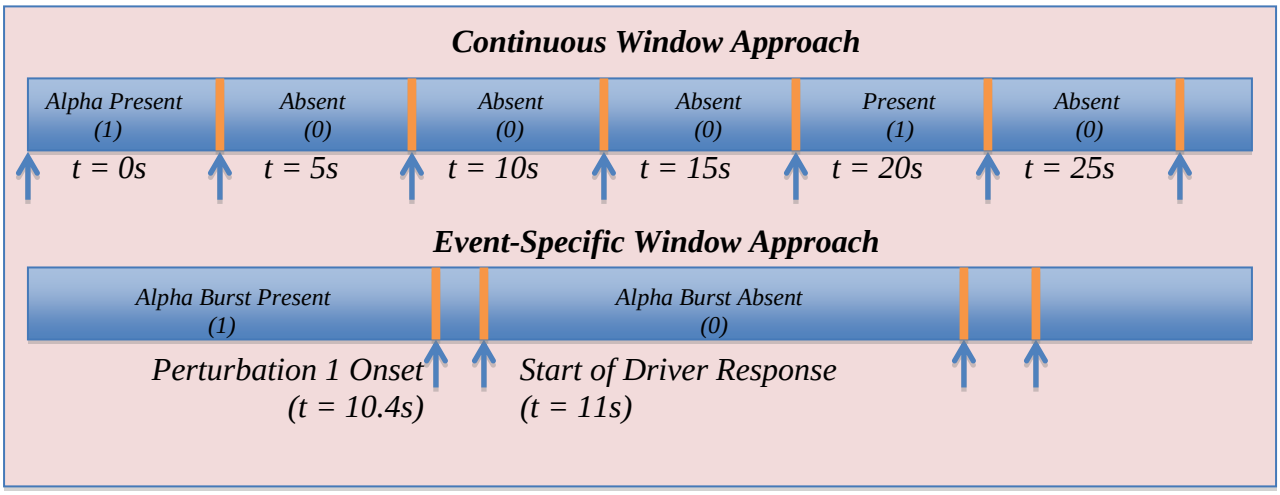

Figure 13. Graphical representation of two approaches to windowing driver performance data.

2.5 Cross Correlations

To analyze inter-subject variability in each metric we used for analysis, we performed multiple one-way analysis of variance (ANOVA) tests on gaze distribution, pupil dilation, standard deviation of lane position (SDLP), and standard deviation of acceleration (SDA). Each ANOVA analysis involved only one of the aforementioned metrics and compared the variability of each subject with respect to the metric being analyzed. To prepare analysis of the correlations between the three sensor modalities, we first had to sync all data streams to a universal clock, eliminating windows that were not in sync among all sensors analyzed. This involved performing linear transformations to the time indices of the data that accounted for both a constant offset time and a linear drift term. In addition, windows were removed from all data streams that were deemed "bad windows" for either the pupil diameter or gaze distribution data.

In order to find the cross-correlation coefficients, linear correlation analysis was performed between each of the eye-tracking and driver performance parameters: gaze distribution, pupil diameter, STDLAT, and SDA. Due to a lack of coinciding alpha bursts with "good windows" of eye-tracking and driver performance data, no cross-correlation coefficients were calculated between alpha bursts and the aforementioned metrics.

3. Results

3.1 Detection of Alpha Bursts

3.3.1 Algorithm Improvement

Figure 14 illustrates the sensitivity and specificity for each channel. The red dot indicates the minimum distance to the vector <1, 1> (located in the top left corner), and therefore corresponds to the optimal EEG channel—Parietal-Occipital 7 (PO7). The real-time implementation of the algorithm with all of the original parameters yielded a sensitivity of 63% and a specificity of 80% for the PO7 channel.

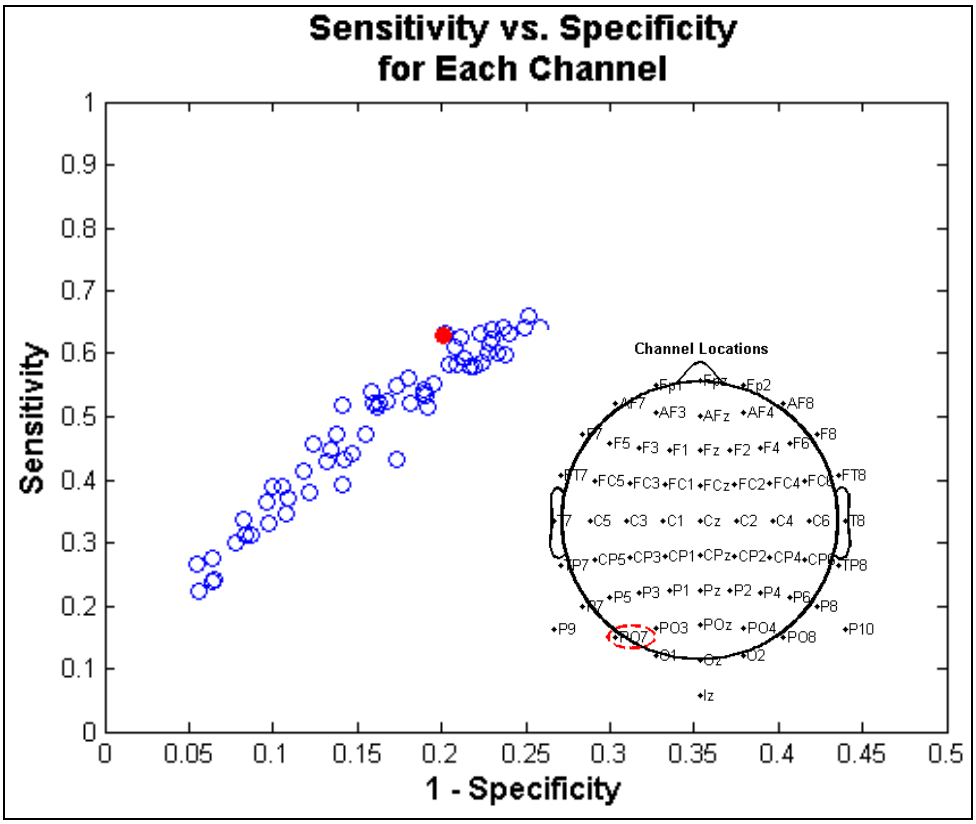

Figure 14. Graphical representation of the average sensitivity and specificity for all participants for each EEG channel, and the corresponding location of each EEG channel. The PO7 channel is red in order to highlight that it is the optimal channel.

Table 1 exhibits the remaining algorithm parameters that were optimized for improved sensitivity and specificity using the training dataset. The overlap between windows did not change through optimization. However, the window length, minimum alpha frequency, and maximum alpha frequency parameters were improved through this optimization.

Table 1. List of the parameters with original values and optimized values shown. The sensitivity and specificity (from training data) for each parameter before and after optimization are also included.

Parameter	Original Value	Original Sensitivity	Original Specificity	Optimal Value	Optimal Sensitivity	Optimal Specificity
Window Length	1 s	63%	80%	1.4 s	66%	76%
Overlap (% Window)	75%	64%	76%	75%	64%	76%
Minimum Alpha Frequency	7 Hz	65%	77%	8.1 Hz	65%	81%
Maximum Alpha Frequency	13 Hz	64%	77%	12.1 Hz	67%	78%

3.3.2 Testing and Validation

Table 2 displays the sensitivity, specificity, and performance coefficients of the algorithm in its original state, when it is implemented in real time with the original parameters, and when it is implemented in real time with the optimized parameters. The original algorithm yielded a high specificity, but low sensitivity. Implementation of the algorithm in real time with the original parameters caused the specificity to decrease and the sensitivity and the performance coefficient to increase. Optimization of individual parameters yielded an improvement in the sensitivity and specificity of the algorithm.

Table 2. Sensitivity, specificity, and performance coefficients (from testing data) for all three iterations of the alpha burst detection algorithm are shown.

	Original Algorithm	Original Algorithm Implemented in Real-Time	Optimized Algorithm Implemented in Real-Time
Sensitivity	36%	67%	69%
Specificity	93%	78%	80%
Performance coefficient	71%	73%	75%

As described above, we performed two-sample t-tests on the frequency of alpha bursting in each dataset. Below are the p-values for the hypothesis that the frequency of alpha bursting in two datasets is equivalent (i.e., the below p-values are indicative of the probability that any observed difference in the frequency in alpha bursting was due to random chance.)

- Training to Validation: 0.53
- Testing to Validation: 0.75

The p-values generated by the t-tests do not disprove the hypothesis that the three datasets are statistically identical.

3.4 Eye-tracking

Figure 15 is a pictorial representation of the change in gaze distribution across a complete test of a single subject. The left histogram shows the beginning third of the data, and the right histogram shows the last third of the data. The horizontal plane is a representation of the simulation field of view, separated into super-pixels. The vertical bars represent the number of data points at which the eye point-of-regard was in that super-pixel. The temporal change in spatial gaze distribution is obvious for each subject, but differs significantly between subjects.

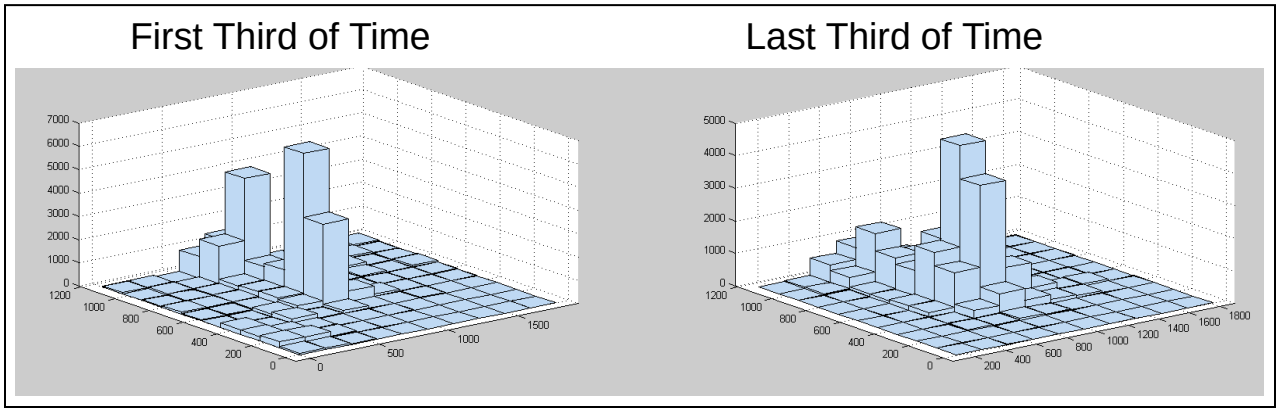

Figure 15. Gaze distribution difference over simulation duration. The horizontal plane is a representation of the simulation field of view, separated into super-pixels. The vertical bars represent the number of data points at which the eye point-of-regard was in that super-pixel.

3.5 Cross Correlations

The analysis performed was limited to gaze distribution, pupil diameter, standard deviation of lane position, and standard deviation of acceleration. The limited analysis was due to limited overall data quantity. Specifically, this was the result of both malfunctions in the eye-tracking system and an inconsistent clock among sensor modalities. These problems yielded large regions of missing and incomparable data among the three sensor systems. This substantially reduced the amount of data available for each modality, and particularly impacted the behavioral analysis. In addition, of the remaining data, there was only a very small portion that was overlapping; thus, we could not complete cross modality comparisons with significant statistical power, one of the initial project goals. Recommendations for improving data quality in future experiments are included in a separate report (*32*). Only the continuous window approach was used for the results detailed below. The primary method of analysis used for these measures was linear correlation analysis.

The R^2 values calculated from the correlation coefficients between eye-tracking and driving metrics are reported in table 3. The majority of the coefficients were insignificant. The significant results, 90% confidence (yellow) and 95% confidence (green), indicated very low correlation coefficients. No single subject or combination of parameters yielded a statistically significant p-value. Inter-subject variation seems to dominate the results.

Table 3. R^2 values for all correlation combinations. The green cells have 95% confidence (p<=0.05) and the yellow cells have 90% confidence (p<=0.1).

Subject	Gaze-Pupil	Gaze-SDA	Gaze-SDLP	Pupil-SDA	Pupil-SDLP	SDA-SDLP
11	0.0000	0.0047	0.0000	0.0007	0.0073	0.0069
12	0.0905	0.0012	0.0120	0.0050	0.0233	0.0049
13	0.0190	0.0136	0.0000	0.0153	0.0002	0.0001
15	0.0085	0.0032	0.0015	0.0046	0.0606	0.0044
16	0.0001	0.0005	0.0596	0.0026	0.0017	0.0004
17	0.0114	0.0010	0.0005	0.0006	0.0005	0.0009
18	0.0015	0.0004	0.0039	0.0001	0.0010	0.0130

Note: Gaze = saccade velocity measure (eye measure), Pupil = Low frequency pupil diameter (eye measure), SDA = standard deviation of acceleration (driving measure), and SDLP – standard deviation of lane position (driving measure).

The F statistic for each of the one-way ANOVA tests was large, indicating that the probability that each subject's data (across all sensor modalities) comes from the same distribution is nearly zero. This indicates that non-parametric statistics are necessary in order to combine data across subjects in analyzing correlations.

No analysis could be completed regarding the correlation of alpha bursts with eye data because none of the alpha bursts coincided with "good windows" in the eye-tracking data. Therefore, all of the data containing alpha bursts were thrown out before the correlation analysis.

4. Conclusions

4.1 Detection of Alpha Bursts

By adjusting the noise approximation methods in the algorithm in reference 20 to implement a real-time alpha burst detection algorithm, we were able to contribute to the development of a fieldable, EEG-based drowsiness detector. Since the window length is relatively short in the real-time implementation of the alpha burst detection algorithm, the noise present within each window fluctuates significantly. One might expect this variation in noise to degrade the noise approximation. However, estimating the noise on a window-by-window basis proves to be more adaptable to differences in noise between subjects and with time. The real-time implementation yields a higher performance coefficient than the original algorithm, in addition to being fieldable.

Independently optimizing parameters of the real-time implementation of the alpha burst detection algorithm improves the sensitivity and specificity of the overall algorithm as well. The algorithm performed better on the PO7 channel than on any other channel. This is consistent with the finding that the primary source of the alpha rhythm is in the posterior and occipital regions of the brain (*13*). The optimal alpha frequency range for the algorithm was 8.1–12.1 Hz (changed from 7–13 Hz). These changes reflect the alpha burst frequencies in the ground-truthed data. The

new minimum alpha frequency cutoff is consistent with most views of the alpha frequency range of 8–13 Hz (*13*). The decrease in the upper limit of the alpha frequency indicates that the majority of alpha bursts in this study were contained within the lower alpha band (8–10 Hz). Activity in the lower alpha component is indicative of cognitive processing and mental effort (*35*).

4.2 Cross Correlations

The majority of the correlations between driving data and eye-tracking measures (reported in table 3) were of low confidence. Low confidence, where alpha is defined as 0.05 or greater, is indicative of correlations that cannot be statistically differentiated from the lack of a correlation. While some metrics for some subjects appear statistically significant in our results, they appear to indicate a very weak correlation. Additionally, these low-correlation-high-confidence results appear highly subject-specific. The high inter-subject variability in eye-tracking measures and driving performance, as indicated by ANOVA, partially helps to explain this result. In order to perform further analysis on the universal correlations between these reported metrics, non-parametric statistics must be used to account for inter-personal variation. In additional, a larger quantity of clean data are necessary to obtain resolution with respect to the many low-confidence correlations observed.

With respect to the eye-tracking data, it is apparent that these measures cannot be used exclusively for drowsiness detection. Without specific measures of a subject's position in space relative to the eye-tracking device, head motion can cause significant degradation of data quality. Furthermore, extended periods of eye closure, which are associated with drowsiness, can result in significant data loss. For these reasons, sensor fusion is necessary to compensate for periods of data loss and is the most effective means for the optimization of complex physiological state determination.

4.3 Future Work

Given the limited time-frame, this summer project is a small piece of a larger effort to accurately predict degradation of driving performance due to drowsiness. In order to further improve the alpha burst detection algorithm, the integration of multiple EEG channels should be investigated. A central decision engine could treat each channel as an individual sensor, which would yield more accurate results than would a single channel. In this distributed sensor scheme, the transmitted information to the central decision engine would be on the level of bits per time interval. Therefore, the accuracy of the algorithm would be improved without sacrificing power or bandwidth. This setup also aims to improve the robustness of the detector by giving each alpha burst detector a relatively small weighting in the decision engine algorithm.

With an improved dataset, logistic regression could be used to analyze the correlation of alpha burst presence or absence with the continuous metrics representing driving performance and eye movement. Additionally, one could use paired sample t-tests to test the hypothesis that alpha

burst presence is associated with different mean driving performance, pupil diameter, or gaze distribution. Future analysis could also make use of the event-specific window approach detailed above. This analysis could include the correlations between eye-tracking, driver performance measures, and alpha burst presence with respect to one's reaction time to a perturbation.

The continuation of this project should include the addition of other eye-tracking measures, especially PERCLOS. Additionally, EOG recordings provide several measures like blink amplitude/velocity and saccade velocity, which have the potential to enhance drowsiness assessment and driver performance prediction capabilities. Other measures indicative of the autonomic nervous system like skin conductivity and measures derived from heart rate, or body orientation data are also viable paths forward, but as these parameters were not investigated as part of this HRED study, their inclusion would require further experimentation. A complete assessment of the data and recommendations for future experiments can be found in reference 32.

5. References

1. Dinges, D. F.; Mallis, M. M.; Maislin, G.; Powell, J. W. Evaluation of Techniques for Ocular Measurement as an Index of Fatigue and the Basis for Alertness Management, April 1998.
2. Lin, C. T.; Wu, R. C.; Jung, T. P.; Liang, S. F.; Huang, T. Y. *EURASIP Journal on Applied Signal Processing* **2005**, *19*, 3165–3174.
3. O'Hanlon, J. F. *What is the Extent of the Driving Fatigue Problem? In Driving Fatigue in Road Traffic Accidents, Brussels: Commission of the European Communities*; Report No. EUR6065EN; l9–25, 1978.
4. McDonald, N. *Fatigue, Safety and the Truck Driver*; Taylor & Francis: London, 1984.
5. Home, J. A.; Reyner L. A. Sleep Related Vehicle Accidents. *British Medical Journal* **1995**, *310*, 565–567.
6. Knipling, R. R.; Wang, J. S. Revised Estimates of the U.S. Drowsy Driver Crash Problem Size Based on General Estimates System Case Reviews. In *39th Annual Proceedings, Association for the Advancement of Automotive Medicine*, Chicago, 1995.
7. Maycock, G. Sleepiness and Driving: The Experience of U.K. Drivers. *Accident Analysis and Prevention* **1997**, *29*, 453–462.
8. Wang, J. S.; Knipling, R. R. Single-Vehicle Roadway Departure Crashes: Problem Size Assessment and Statistical Description. U.S. Department of Transportation, National Highway Traffic Safety Administration, 1994.
9. Brown, I. D. Methodological Issues in Driver Fatigue Research. In Hartley, L. (Ed) Fatigue & Driving: Driver Impairment, Driver Fatigue and Driving Simulation, Taylor & Francis, London, 1995.
10. Shafer, J. H. The Decline of Fatigue Related Accidents on the NYS Thruway. In *Proceedings of the Highway Safety Forum on Fatigue, Sleep Disorders and Traffic Safety*, Albany, NY, 1993.
11. Dinges, D. F. An Overview of Sleepiness and Accidents. *Journal of Sleep Research 4: (Supplement 2)* **1995b**, 4–14.
12. Kribbs, N. B.; Dinges, D. F. Vigilance Decrement and Sleepiness. In Harsh, J. R. & Ogilvie, R. D. (Eds.), Sleep Onset Mechanisms. *American Psychological Association*, Washington, DC, pp. 113–125, 1994.

13. Cantero, J. L.; Atienza, M.; Salas, R. M. Human Alpha Oscillations in Wakefulness, Drowsiness Period, and REM Sleep: Different Electroencephalographic Phenomena within the Alpha Band. *Neurophysol Clin* **2002**, *32*, 54–71.

14. Picot, A.; Charbonnier, S.; Caplier, A. On-Line Automatic Detection of Driver Drowsiness Using a Single Electroencephalographic Channel. In *30th Annu. Int. Conf. of the IEEE Engineering in Medicine and Biology Society*, Vancouver, BC: Canada, 2008.

15. Dinges, D. F. PERCLOS: A Valid Psychophysiological Measure of Alertness As Assessed by Psychomotor Vigilance. Federal Highway Administration Tech Brief, Publication No. FHWA-MCRT-98-006) 1998. http://www.fmcsa.dot.gov/documents/tb98-006.pdf.

16. Merritt, S. L. Using Pupillometry to Measure Sleepiness: The Reproducibility, Ultradian Sensitivity and Validity of Outcome Measures. Abstract from Conference]. http://www.nursinglibrary.org/vhl/handle/10755/183410.

17. Ingre, M.; Akerstedt, T.; Peters, B.; Anund, A.; Kecklund, G. Subjective Sleepiness, Simulated Driving Performance and Blink Duration: Examining Individual Differences. *J. Sleep Res.* **March 2006**, *15* (1), 47–53.

18. Purves, D. *Neuroscience*; Fourth ed.; Sunderland, MA: Sinaue Associates, Inc., 2008, 715–717.

19. Makeig, S.; Tzyy-Ping, J. Awareness During Drowsiness: Dynamics and Electrophysiological Correlates. *Canadian Journal of Experimental Psychology* **December 2000**, *54* (4), 266. Academic Search Premier, EBSCOhost (accessed June 18, 2012).

20. Simon, M.; Schmidt, E. A.; Kinces, W. E.; Fritzsche, M.; Bruns, A.; Aufmuth, C.; Bogdan, M.; Rosenstiel, W.; Schrauf, M. EEG Alpha Spindle Measures as Indicators of Driver Fatigue Under Real Traffic Conditions. *Clinical Neurophysiology* **2011**, *122*, 1168–1178.

21. Cantero, L. C.; Atienza, M. Spectral and Topographic Microstructure of Brain Alpha Activity During Drowsiness at Sleep Onset and REM Sleep. *Journal of Phychophysiology* **2000**, *14*, 151–158.

22. Ji, Q.; Lan, P.; Looney, C. A Probabilistic Framework for Modeling and Real-Time Monitoring Human Fatigue. *IEEE Transactions on Systems, Man, and Cybernetics – Part A: Systems and Humans* **September 2006**, *36* (5).

23. Klimesch, W.; Schimke, H.; Pfurtscheller, G. Alpha Frequency, Cognitive Load and Memory Performance. *Brain Topography* **1993**, *5*, 241–251.

24. Kircher, A.; Uddman, M.; Sandin, J. Vehicle Control and Drowsiness. Swedish National Road and Transport Research Institute, VTI meddelande 922A, 2002.

25. Russo, M.; Thomas, M.; Thorne, D.; Sing, H.; Redmond, D.; Rowland, L.; Johnson, D.; Hall, S.; Kirchmar, J.; Balkin, T. Sleep Deprivation Related Changes Correlate with Simulated Motor Vehicle Crashes. In R. Carroll (Ed.) Ocular Measures of Driver Alertness. *Technical Conference Proceedings* (FHWA Technical Rep. No. FHWA-MC-99-136), Washington DC, Federal Highway Administration, Office of Motor Carrier and Highway Safety, 119–127, 1999.

26. Jain, S.; Siegle, G. J.; Gu, C.; Moore, C. G.; Ivanco, L. S.; Jenning, J. R.; Steinhauer, S. R.; Studenski, S.; Greenamyre, J. T. Autonomic Insufficiency in Pupillary and Cardiovascular Systems in Parkinson's Disease http://www.ncbi.nlm.nih.gov/pmc/articles/PMC3034773/. *Parkinsonism Relat Disord.* **February 2011**, *17* (2), 119–122.

27. Van Orden, K. F.; Jung, T. P.; Makeig, S. *Biological Psychology* **2000**, *52*, 221–240.

28. Ingre, M.; Akerstedt, T.; Peters, B.; Anund, A.; Kecklund, G. Subjective Sleepiness, Simulated Driving Performance and Blink. *J. Sleep Res.* **2006**, *15*, 47–53.

29. Liu, Charles C.; Hosking, Simon G.; Lenné, Michael G. Predicting Driver Drowsiness Using Vehicle Measures: Recent Insights and Future Challenges. *Journal of Safety Research* **2009**, *40* (4), 239–245. Academic Search Premier, EBSCOhost (accessed June 18, 2012).

30. Hugemann, W. Driver Reaction Times in Road Traffic, 06–07 Sept. 2002. (From EVU 2002 in Slovenija, Portoroz) http://www.hugemann.de/pdf/evu_2002_reaction_english.pdf.

31. NCSDR/NHTSA Expert Panel on Driver Fatigue and Sleepiness, Drowsy Driving and Automobile Crashes. http://www.nhtsa.gov/people/injury/drowsy_driving1/drowsy.html.

32. Silversmith, D.; Perkons, N.; Jordan, K.; Nothwang, W.; Brooks, J.; Hairston, W.; Kerick, S.; Lance, B.; McDowell, K. *Multi-modality Physiological Monitoring of Drowsiness—Recommendations for Future Experiments*; ARL-MR-0833; U.S. Army Research Laboratory: Adelphi, MD, December 2012.

33. Swartz Center for Computational Nureoscience. EEGLAB. http://sccn.ucsd.edu/eeglab (accessed August 2012).

34. Pereda, E.; Gamundi, A.; Rial, R.; Gonzlez, J. Non-linear Behavior of Human EEG: Fractal Exponent Versus Correlation Dimension in Awake and Sleep Stages. *Neuroscience Letters* **1998**, *250*, 91–94.

35. Lin, S. T.; Tan, Y. Y.; Chua, P. Y.; Tey, L. K.; Ang, C. H. PERCLOS Threshold for Drowsiness Detection during Real Driving. *Journal of Vision* **August 13, 2012**, *12* (9), article 546.

List of Symbols, Abbreviations, and Acronyms

ANOVA	analysis of variance
ASD	amplitude spectral density
EEG	electroencephalography
EOG	electrooculography
FWHM	full width at half maximum
GAZEDIS	gaze distribution
HRED	Human Research and Engineering Directorate
KSS	Karolinska Sleepiness Scale
NTSB	National Transportation Safety Board
PO7	Parietal-Occipital 7
PVT	psychomotor vigilance test
SDA	standard deviation of acceleration
SDLP	standard deviation of lane position
STDLAT	standard deviation of lateral lane position

NO. OF COPIES	ORAGANIZATION
1 (PDF only)	DEFENSE TECHNICAL INFORMATION CTR DTIC OCA 8725 JOHN J KINGMAN RD STE 0944 FORT BELVOIR VA 22060-6218
1	DIRECTOR US ARMY RESEARCH LAB IMAL HRA 2800 POWDER MILL RD ADELPHI MD 20783-1197
1	DIRECTOR US ARMY RESEARCH LAB RDRL CIO LL 2800 POWDER MILL RD ADELPHI MD 20783-1197
5	US ARMY RSRCH LAB ATTN RDRL-HRS-C W D HAIRSTON ATTN RDRL-HRS-C K MCDOWELL ATTN RDRL-HRS-C S KERICK ATTN RDRL-HRS-C J BROOKS ATTN RDRL-HRS-C B LANCE ABERDEEN PROVING GROUND MD 21005
6	US ARMY RSRCH LAB ATTN RDRL CII A J TWIGG ATTN RDRL CIN B SADLER ATTN RDRL SER L A WICKENDEN ATTN RDRL SER L B PIEKARSKI ATTN RDRL SER L W NOTHWANG ATTN RDRL SER L J CONROY ADELPHI MD 20783-1197
1	CALIFORNIA INSTITUTE OF TECHNOLOGY ATTN MC 305-16 E WOLFF 1200 E CALIFORNIA BLVD PASADENA CA 91125
1	UNIVERSITY OF PENNSYLVANIA MULTIMEDIA AND NETWORKING LABORATORY ATTN A KOPPEL 306 MOORE 200 SOUTH 33RD STREET PHILADELPHIA, PA 19104
1	UNIVERSITY OF CALIFORNIA BERKELEY ATTN DAN CALDERONE 337 CORY HALL BERKELEY, CA 94720-1772
4	HARVARD UNIVERSITY ATTN NICHOLAS PERKONS, 509 KIRKLAND M.C. 95 DUNSTER ST. ATTN PROF. SUJATA BHATIA, PIERCE HALL 206C, 29 OXFORD STREET ATTN PROF. DAVID MOONEY, PIERCE HALL 325, 29 OXFORD STREET ATTN PROF. ROBERT LUE, BIOLABS 1081, 16 DIVINITY AVENUE CAMBRIDGE, MA 21038
1	CEDARVILLE UNIVERSITY ATTN MICHAEL COMPARETTO 251 N. MAIN STREET # 2554, CEDARVILLE, OH 45314
1	PRINCETON UNIVERSITY YUAN CHEN 1471 FRIST CAMPUS CENTER PRINCETON, NJ 08544
1	VISHNU GANESAN 2280 SOUTH OVERLOOK ROAD, CLEVELAND OH, 44106
1	KESSHI JORDAN 14526 MACCLINTOCK DR. GLENWOOD, MD 21738
1	KATHRYN SCHNEIDER 8204 BALTIMORE AVE APT#1026C COLLEGE PARK, MD 20740
1	MICHAEL ROBERTS 12608 IVYSTONE LANE LAUREL, MD 20708
1	CORDELL REID 8531A GREENBELT RD, APT 202, GREENBELT MD 20770

NO. OF
COPIES ORAGANIZATION

1 TRISTAN HELMS
928 S STATE ST APT 4
ANN ARBOR, MI 48104

1 RAINER & PATRICIA PERKONS
30 DICKINSON ROAD
KENDALL PARK, NJ 08824

1 JAMES & MARIE DACEY
170 PACIFIC AVENUE
STATEN ISLAND, NY 10312

1 NAVAL SURFACE WARFARE CENTER
ATTN JESSE CAMPBELL, K74, 5370
MARBLE ROAD, SUITE 143
DAHLGREN, VA 22448-5165

TOTAL: 32 (1 ELEC, 31 HCS)

INTENTIONALLY LEFT BLANK.